Characterization of Electrodes for Kilohertz Electrical Stimulation

A Thesis
Presented to
The Academic Faculty

by

Brian Kim

In Partial Fulfillment
of the Requirements for the Degree
Bachelor of Science in Biomedical Engineering in the
Wallace H. Coulter Dept. of Biomedical Engineering

Georgia Institute of Technology
May 2017

Characterization of Electrodes for Kilohertz Electrical Stimulation

Approved by:

Dr. Robert Butera, Advisor
Wallace H. Coulter Dept. of Biomedical Engineering
School of Electrical/Computer Engineering
Georgia Institute of Technology

Dr. Pamela Bhatti
School of Electrical/Computer Engineering
Georgia Institute of Technology

Date Approved: [Date Approved by Committee]

Table of Contents

ACKNOWLEDGEMENTS

I wish to thank my mentor Dr. Yogi A. Patel who has supported me throughout my entire research career and Dr. Robert J. Butera, research advisor, who has allowed me to conduct research and learn everything I know now. Last but not least, I would like to thank William S. Rountree, a fellow undergraduate student who had so much promise as a researcher and was a great friend.

Some of the following passages have been quoted verbatim from the following sources:

Patel Y.A, Kim B.S, Rountree W.S, Butera R.J (2016*), Kilohertz Electrical Stimulation Nerve Conduction Block: Effects of electrode surface area*. In press for IEEE Transactions on Neural Systems & Rehabilitation Engineering

Patel Y.A, Kim B.S, Rountree W.S, Butera R.J (2016*), Kilohertz Electrical Stimulation Nerve Conduction Block: Effects of electrode materials*. Under review

SUMMARY

Kilohertz electrical stimulation (KES) induces repeatable and reversible conduction block of nerve activity and is a potential therapeutic option for various diseases and disorders resulting from pathological or undesired neurological activity. However successful translation of KES nerve block to clinical applications is stymied by many unknowns such as the relevance of the onset response, acceptable levels of waveform contamination, and optimal electrode characteristics. We investigated the role of electrode geometric surface area and electrode contact material on the KES nerve block threshold using 20 and 40 kHz current-controlled sinusoidal KES. Electrodes were electrochemically characterized and used to characterize typical KES waveforms and electrode charge characteristics. KES nerve block amplitudes, onset duration, and recovery of normal conduction after delivery of KES were evaluated for effective KES nerve block. Results from this investigation demonstrate that increasing electrode geometric surface area provides for a more efficient KES nerve block and different materials has no effect on KES nerve block thresholds. Reductions in block threshold by increased electrode surface area were found to be KES frequency dependent, with block thresholds reduced by >2x with 20 kHz KES waveforms and >3x for 40 kHz KES waveforms.

CHAPTER 1

INTRODUCTION

Kilohertz electrical stimulation (KES), also referred to as kilohertz high frequency alternating current (KHFAC) or high frequency alternating current (HFAC) throughout the literature, is a safe and reversible method to reduce or block propagating neural activity in peripheral nerves (2015, Bhadra et al). KES nerve block has been demonstrated in a variety of animal models and nerve diameters, including sea slugs [1], frogs [2], [3], rats [4]–[6], cats [7], [8] dogs [9], goats [10], pigs [11], and non-human primates [12]. These studies have demonstrated the ability to achieve a quick, reversible, localized block of peripheral nerve activity. Peripheral nerve conduction block has many potential applications - as an experimental tool, where it can replace permanent traditional methods such as nerve transections as well as in the clinic, where it may be a potential treatment option for various diseases and disorders such obesity[11], and chronic inflammation[13].

Achieving a successful localized, repeatable, and robust nerve block of propagating activity requires appropriate design and fabrication of the neural interface to be used. Several publications have reported nerve cuff electrode designs optimized for either stimulation or recording of peripheral nerve activity. Such optimizations include specific fascicles stimulation [14], chronic safety [15], and stimulation thresholds reduction [5],[16]. In contrast, very few studies have specifically investigated the effect of neural interface characteristics on the block threshold. The few studies that exist have characterized the effects of different inter-polar distances [17] and multipolar configurations [18]. Furthermore, almost all published results have reported the use of different interfaces (as shown in Table I). These reports differ in electrode type, materials, and geometry, as well as animal model and target nerve, with many publications missing sufficient details to enable valuable comparison.

The focus of this thesis is to systematically evaluate the effect of electrode contact geometric surface area (GSA) and electrode contact material, if any, on KES nerve block

Table I
Reported electrode specifications for KES nerve block (Adapted from [21] with permission).

Publication	Configuration	Contacts	Conductor	Species
Cattell 1935 [23]	ND	Wires	Ag/Calomel	Frog
Rosenblut 1939 [21]	Bipolar	Wires	Ag|Ag/Cl	Cat
Reboul 1939 [24]	Bipolar	Wires	Ag|Ag/Cl	Cat
Tanner 1962 [25]	Bipolar	ND	Pt	Frog
Woo 1964 [26]	Bipolar	ND	ND	Frog/Cat
Baratta 1989 [27]	Tripolar	Wires	SS	Cat
Bowman 1986 [28]	Bipolar	Wire	Pt	Cat
Kilgore 2004 [2]	Bipolar	Wire	Pt	Frog
Tai 2004 [29]	Tripolar	Wires	SS	Cat
Bhadra 2005 [20]	Tripolar	Pads	Pt	Rat
Williamson 2005 [5]	Tripolar	Wires	SS	Rat
Bhadra 2005 [20]	Tripolar	Pads	Pt	Rat
Bhadra 2006 [7]	Tripolar	Pads	Pt	Cat
Miles 2007 [30]	Tripolar	Pads	Pt	Rat
Boger 2008 [31]	Tripolar	ND	ND	Cat
Joseph 2007 [32]	Bipolar	Wires	Ag|Ag/Cl	Sea Slug
Ackermann 2009 [21]	Bipolar	Pads	Pt	Rat
Ackermann 2010 [22]	Bipolar	Pads	Pt	Rat
Ackermann 2010 [33]	Bipolar	Pads	Pt	Rat
Gerges 2010 [34]	Bipolar	Pads	Pt	Rat
Ackermann 2010 [35]	Bipolar	Wires	W	Rat
Ackermann 2011 [36]	Monopolar	Pads	Pt+Ag|Ag/Cl	Rat
Ackermann 2011 [12]	Bipolar	Pads	Pt	Rat
Ackermann 2011 [37]	Monopolar SINE	Pads	Pt	Rat
Ackermann 2011 [3]	Bipolar	Pads	Pt	Non-Human Primate
Joseph 2009 [1]	Bipolar	Wires	Ag|Ag/Cl	Sea Slug
Joseph 2011 [3]	Bipolar	Wires	Ag|Ag/Cl	Sea Slug
Liu 2013 [38]	Bipolar	Wires	Ag|Ag/Cl	Frog
Patel 2015 [4]	Tripolar	Pads	Pt/Ir	Rat
Yang 2016 [39]	Tripolar	ND	ND	Frog
Patel 2016 [40]	Bipolar	Pads	Pt/Ir	Rat

Sine = Separated Interface Nerve Electrode, ND = Not Described

thresholds. The electrode contacts were cut off of metal sheets, and then experiments were carried out to investigate the effects of contact GSA and material on KES block thresholds.

This thesis interpolates material from two papers by the author (BSK) [42,43]. Chapter 2, 3, 4, and 5 uses material from references [42] and [43], coauthored with Dr. Yogi A. Patel (YAP) and Dr. Robert Butera (RJB) for both [42,43], and William S. Rountree (WSR) for [42]. Some material from each of these papers has also been incorporated into this introductory chapter and the summary.

For [42], YAP, BSK, and WSR designed and conceived the study. BSK and YAP performed experiments. WSR, BSK, YAP, and RJB analyzed data. BSK and WSR fabricated electrodes. WSR and YAP conducted electrochemical characterization experiments. YAP, BSK, WSR, and RJB wrote the manuscript.

For [43], YAP designed and conceived the study. BSK and YAP performed experiments. BSK, YAP, and RJB analyzed data. BSK fabricated electrodes. YAP conducted electrochemical characterization experiments. YAP, BSK, and RJB wrote the manuscript.

CHAPTER 2

METHODS AND MATERIALS

Animal Preparation

All animal research was approved by the Georgia Institute of Technology Institutional Animal Care and Use Committee. Experiments were conducted on tibial nerves from in vivo urethane-anesthetized rats (377.3 ± 72g, n = 6 males for GSA) (384 ± 51g, n = 12 for materials). Animals were briefly anesthetized using isoflurane in oxygen (5%, 1 liter/min flow rate) prior to delivery of urethane (IP, 1.2 g/kg in 0.9% saline). Anesthetic depth was evaluated 60 - 90 minutes post-injection by pinching the rear footpad and supplemental urethane (0.12 mg/ml) was delivered as necessary until the reflex withdrawal was eliminated. After reaching surgical depth, the animal's back was shaved from the lumbar section down to the distal end of the gastrocnemius muscle. The animal's foot was magnetically clamped to the surgical table to minimize motion during experimental trial. An incision approximately 1 - 1.5 cm in length was made along the length of the biceps femoris muscle and the sciatic nerve exposed via blunt dissection. The tibial branch of the sciatic nerve was identified and isolated from the sciatic notch down to the gastrocnemius muscle under a high magnification dissection scope. The common peroneal, sural, and collateral branches of the sciatic were cut to minimize off-target stimulation. Normal rat ringer's solution [44] was applied throughout the experiment to prevent muscle and nerve tissue dehydration. The animal's body temperature was monitored and maintained at 37 - 40˚C with a rectal temperature probe (Model BAT-12, Physitemp Instruments, Clifton, NJ) and warming pad (COM- 11289, SparkFun Electronics, Niwot, CO). Preparations lasted 5 - 6 hours after which animals were euthanized via an IP injection of pentobarbital-based euthanasia drug (0.5 ml/kg, IP). All experiments were conducted at room temperature.

Electrophysiology Setup

The proximal end of the exposed sciatic nerve was stimulated using a bipolar cuff electrode made in-house. Two braided stainless steel wires (#793500, A-M Systems, Sequim, WA) separated by 1 mm were deinsulated and threaded through silicone tubing (#807600, A-M Systems, Sequim, WA). A second bipolar stimulation cuff electrode was placed approximately 0.2 cm distal to the block electrode in all experiments for delivery of distal test stimuli. The spacing was determined by the availability of space on the rat's tibial nerve. Distal test stimuli verified that KES nerve block was localized to the site of the block electrode and did not cause neuromuscular fatigue or neurotransmitter depletion. Spacing between the proximal stimulation and block electrodes was approximately 1 cm in all experiments. EMG activity was differentially measured from the gastrocnemius muscles using bipolar fine wire electrodes (Cooner Wire No. AS631, Chatsworth, CA). EMG measurements were filtered (100 - 300 Hz) and gained (1000x, Brownlee Precision Model 440, San Jose, CA) before being digitized at a rate of 20 kHz using The Real-Time eXperiment Interface (RTXI, http://www.rtxi.org, Patel et al 2016, in review at PLOS Comp. Biol.) with a PCI-6036E data acquisition card (National Instruments, Austin, TX). A stainless steel wire was inserted into the contralateral gastrocnemius muscle and connected to the surgical air table to electrically ground the animal, with the surgical table grounded to the amplifier (building supply ground). Figure 1B shows the complete experiment setup.

Table II
Ideal and Actual electrode contact dimensions and geometrics. (Adapted from [42]).

Ideal Contact Dimensions (mm)	0.50 x 0.50	0.50 x 1.00	0.50 x 2.00
Actual Contact Dimensions (mm)	0.50 x 0.50 ± 0.01	0.50 x 1.00 ± 0.01	0.50 x 2.00 ± 0.03
Ideal Contact GSA (cm^2)	0.0025	0.0050	0.0100
Actual Contact GSA (cm^2)	0.0025	0.0050	0.0103
Mean Impedance at 1 kHz (kΩ)	5.54 ± 1.60	2.56 ± 0.60	1.06 ± 0.10
Number of measurements (n)	6	7	7

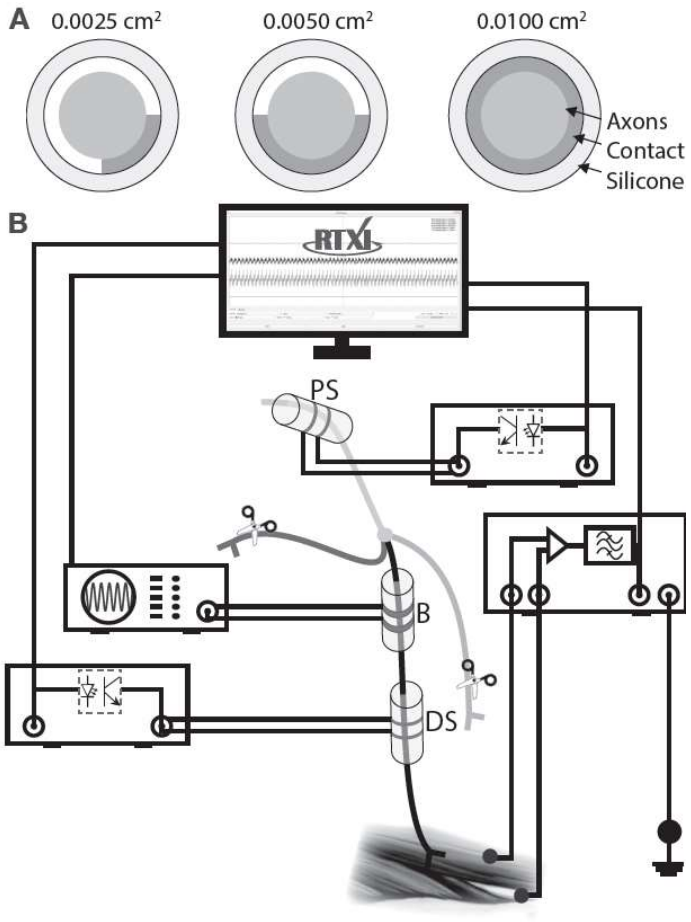

Figure 1. Electrophysiology setup and electrode configurations. (A) Illustration of increasing nerve coverage with increasing contact GSA. (B) The nerve was electrically stimulated at the proximal and distal ends using bipolar cuff electrodes. EMG activity was measured from the gastrocnemius muscle using intramuscular fine wire electrodes. KES nerve block was delivered proximal to the distal stimulation electrode using a bipolar cuff electrode. Timing and duration of stimulation events, along with measurement of activity was achieved with RTXI. PS = proximal stimulation electrode, B = Block electrode, DS = distal stimulation electrode. (Adapted from [42]).

Electrode fabrication (Geometric Surface Area)

Block of the tibial nerve was achieved using Pt/Ir (90/10, 25.4 μm thick) contact pads (ESPI Metals, Ashland, OR) spot-welded to braided stainless steel wire. Contact pads were cut and measured under a high resolution microscope with digital calipers (Table II, measurement error = 0.01), wrapped around the tibial nerve under a dissection microscope, and insulated using silicone (Kwik-Cast, WPI, Sarasota, FL). The width of

all contacts was 0.5 mm. Contact lengths were chosen to provide ≈90 ˚, ≈180 ˚, and ≈360 ˚ coverage based upon a tibial nerve diameter of 2.0 - 2.1 mm [45]. Actual contact GSAs were calculated using measured mean contact dimensions. Impedance measurements were made at 1 kHz in room temperature saline stirred at a constant rate. Values shown are mean ± standard deviation. All calculations requiring contact GSA were conducted using ideal values.

Electrode fabrication (Materials)

Block of the tibial nerve was achieved using SS, Pt, Pt/Ir (90/10), TiN-Pt, and TiN-PtIr (90/10) contact pads (25.4 μm thick, ESPI Metals, Ashland, OR). The length and width of all contacts was 2.0 mm and 0.5 mm, respectively. Electrode contact geometric surface areas (GSAs) were calculated to be 0.01 ± 0.0002 cm^2. This geometry provided complete circumferential coverage of the tibial nerve (Fig. 1A, circumference 2.0 - 2.1 mm [45]), which is critical for minimizing the KES nerve block threshold (Patel et al. 2016, in review IEEE TNSRE). Contact pads were cut and measured under a high-resolution microscope with digital calipers (measurement error = 0.01 mm), spot welded to braided (7-strand) stainless steel wire, and wrapped around the tibial nerve under a dissection microscope, and insulated using silicone (Kwik-Cast, WPI, Sarasota, FL). TiN coated electrodes were fabricated by adhering spot welded Pt and PtIr contacts on a 4 inch silicon wafer using parafilm. Spot-welded leads were insulated with an additional layer of parafilm to prevent deposition of TiN onto lead wires. Porous TiN was sputtered (AJA Magnetron Sputter System, Scituate, MA) onto the exposed contact surfaces at a rate of 7.5 nm/min under a base pressure of 105 Torr and Ar and N2 gas flow rates of 180 and 240 sccm, respectively. These parameters provided a 200 nm layer of TiN on Pt and PtIr contacts.

Nerve Activation and KES Block

Constant current pulses (0.3-0.5 mA_{peak}, 0.2 ms, 1 Hz) were generated using the RTXI signal generator module for proximal stimulation and an optically isolated constant

current stimulator (DS3, Digitimer, Ft. Lauderdale, FL) for distal stimulation. Proximal stimulation pulses were optically-isolated using linear stimulus isolators (A395, WPI, Sarasota, FL). The KES waveform (current-controlled, continuous sinusoid) was generated using a floating current source function generator (Model 6221, Keithley Instruments, Inc, Clevelend, OH). The 2.1 mA_{peak} and 21.0 mA_{peak} ranges were used for the 20 kHz and 40 kHz KES trials, respectively. Direct current contamination of the KES waveform was randomly measured with a 10 Ω sense resistor in series with the return electrode and found to be 150 - 500 nA. All stimulus isolation units used were calibrated prior to each experiment and output offsets zeroed by visualization on an oscilloscope. Timing control of stimulation equipment was achieved by using digital I/O triggers generated from RTXI.

Experimental Protocols

The first trial was conducted to determine the block threshold with a given electrode and KES frequency (as previously described in [4]). The sciatic nerve was stimulated at 1 Hz using the proximal stimulation electrode to elicit supramaximal EMG activity in the gastrocnemius muscle. The threshold was found by increasing the amplitude of the KES waveform in 0.1 mA_{peak} increments until complete block was achieved. Complete block was achieved only when the RMS voltage of the EMG measurement was equivalent to that of the measurement noise. The second trial was conducted at the empirically determined block threshold, with approximately 3 - 5 minutes between each trial to ensure nerve's full recovery. In each trial, a total of 100 stimulation pulses were delivered to the nerve. The initial 21 stimulation pulses were delivered to the nerve to capture pre-KES EMG activity. KES was delivered to the nerve 900 ms after the 21st stimulation pulse at either 20 or 40 kHz with the predetermined block threshold. Test pulses were delivered to the nerve while delivery of KES nerve block for continuous assessment of KES nerve block efficacy. The KES waveform was automatically turned off after 60 seconds (60 stimulation pulses) with continued nerve stimulation to measure post-KES EMG activity (18 stimulation pulses).

Data Analysis

All data were analyzed with MATLAB. EMG recordings were detrended and windowed (10 ms bins) to capture evoked EMG activity. The stimulus trigger was used to define the EMG window's left edge. An additional 10 ms window was used to capture baseline noise prior to stimulus delivery. The windowed data was full-wave rectified and the root mean square (RMS) voltage used as a metric for evaluating nerve and muscle activation as well as KES nerve block. The noise RMS voltage was subtracted from the EMG RMS voltage to reduce variance introduced by noise and differences in electrical coupling between experimental setups. Onset artifacts were identified by comparing the RMS voltage of a moving 10 ms window to pre-KES RMS noise values. Evoked EMG latencies were calculated by subtracting the time of the stimulation trigger from the time of the evoked EMG response. Recovery times were measured as the time between turning of KES and recovery of evoked EMG magnitudes to 90% of pre-KES values. All box plots show the population mean (center black bar), 95% confidence interval (white region), and one standard deviation (gray region).

CHAPTER 3

RESULTS

Geometric Surface Area

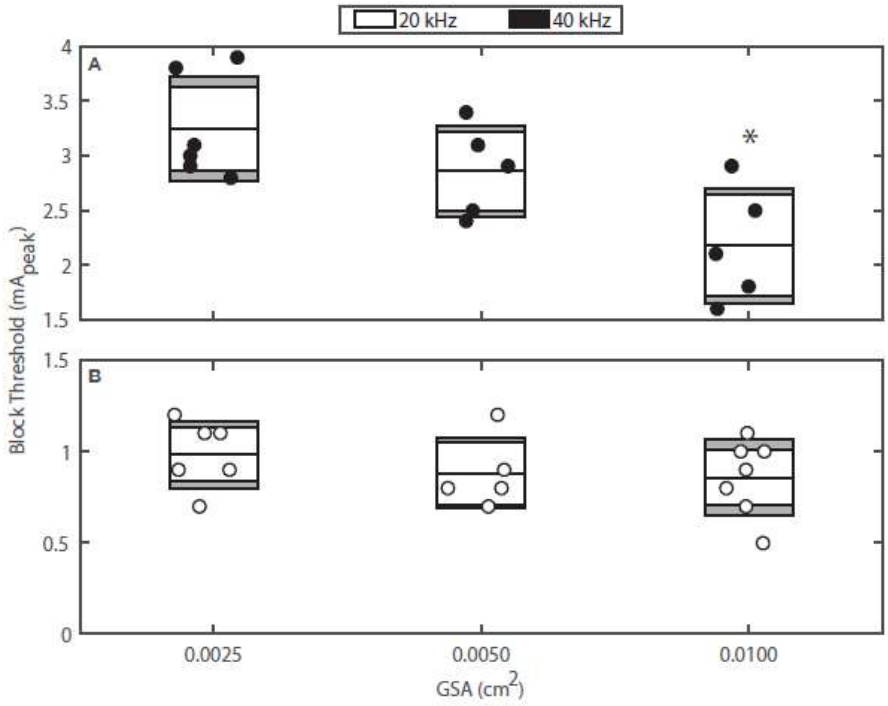

Figure 2. KES block thresholds as a function of contact GSA for 20 and 40 kHz KES nerve block. Each circle represents an individual trial at one KES frequency. Each contact GSA group was found to be normally distributed with the equal variances (Bartlett's statistic, p_{20kHz} = 0.96, p_{40kHz} = 0.91). A one-way analysis of variance did not detect any significance between the mean 20 kHz block thresholds at all contact GSAs ($p < 0.05$), however did reveal a significant difference between the mean 40 kHz block thresholds for 0.0025 cm^2 and 0.0100 cm^2 contact GSAs ($p = <0.05$). (Adapted from [42]).

Increased GSA reduces KES block thresholds

Block thresholds are the primary metric reported by most KES nerve block studies. KES nerve block thresholds reported in this report (Figure 2) demonstrate an inverse relationship with contact GSA; block thresholds decrease as contact GSA increases. Decreases in mean block threshold were not significant with 20 kHz KES waveforms, in contrast to the significant decreases seen with 40 kHz KES waveforms (Figure 2).

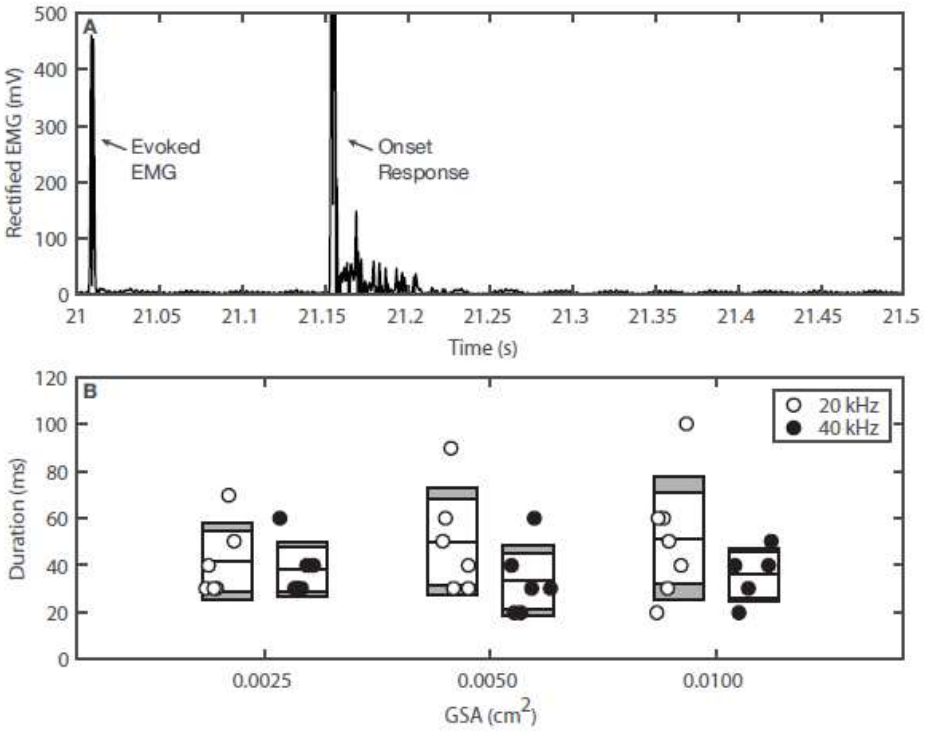

Figure 3. Rectified EMG onset artifact durations. **(A)** Rectified EMG onset artifacts always followed the 21st evoked-EMG response. The onset artifact consists of a large, high-frequency transient spike in measured EMG activity followed by a brief period of spontaneous activation, followed by complete KES nerve block. **(B)** The width of the windows rectified EMG onset artifact is used to represent the duration of the onset artifact as a function of contact GSA and KES frequency. (Adapted from [42]).

Increased GSA does not alter post-KES nerve block characteristics

The clinical utility of KES nerve block may be affected by the onset response, changes in normal nerve conduction, as well as recovery of normal conduction after KES is turned off. The onset response durations (Figure 3) were quantified as a function of KES frequency and contact GSA. No consistent difference was observed in onset duration as a function of contact GSA. Changes in EMG activation (Figure 4) were used as a proxy to assess nerve conduction latencies pre- and post-KES nerve block. Although mean post-KES nerve block EMGs are reduced for all groups, significant variability exists, leading to no consistently identifiable change in EMG activation as a function of KES frequency or contact GSA. Nerve conduction latencies increased after delivery of KES nerve block but no consistent and reproducible change was observed. Mean post- KES latencies increase and demonstrate a wider distribution post-KES. There is no dependence upon contact GSA or KES frequency, however. Normalized

EMG pre- and post- KES nerve block were used to quantify changes in the quality of recovered nerve activity after 60 seconds of complete and effective block (Figure 5). Finally, increasing contact GSAs decreased recovery times for 20 kHz KES trials. This effect however, is not observed for 40 kHz KES trials.

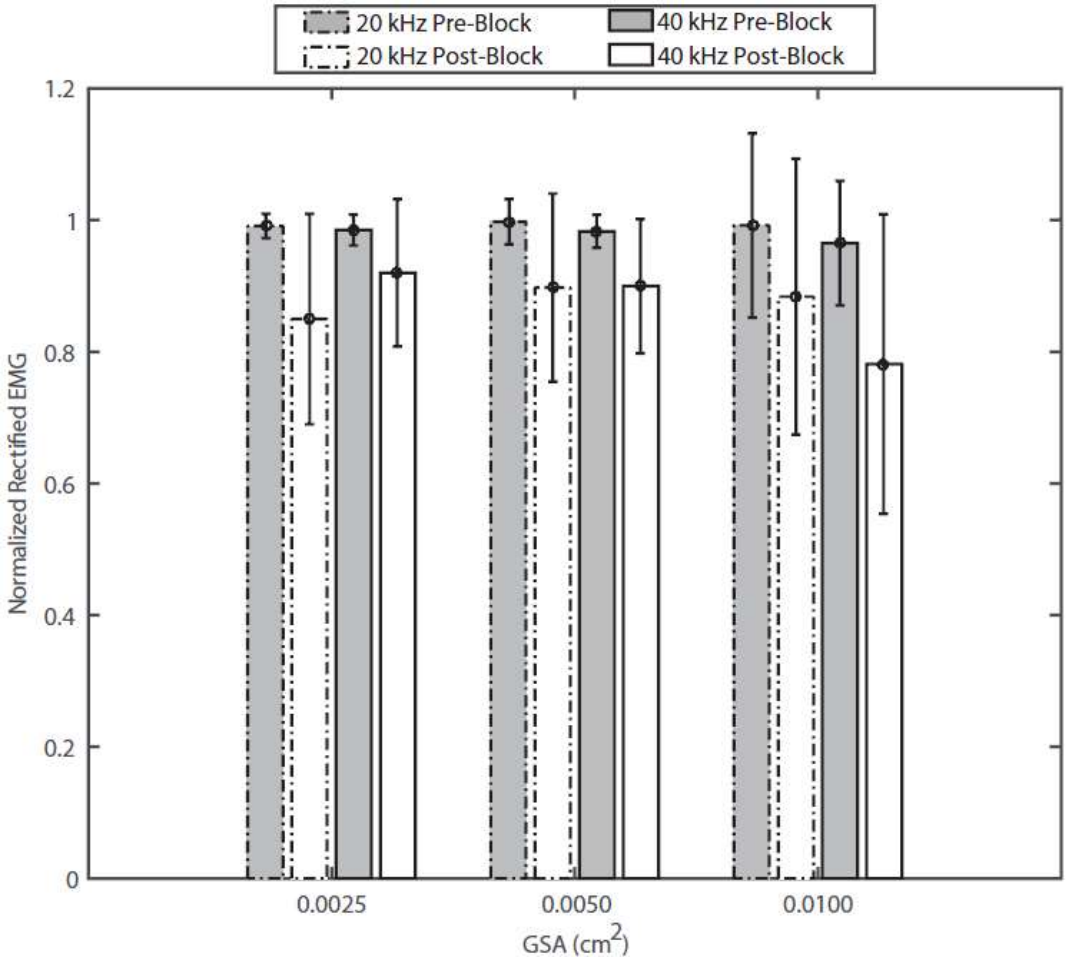

Figure 4. Normalized rectified EMG before and after delivery of KES nerve block. Gray and white bars represent pre- and post-KES nerve block EMG values. Dashed and solid line boxes represent trials using 20 kHz and 40 kHz, respectively. One-way analysis of variance demonstrated no significant difference in pre- and post-block EMG as a function of contact GSAs. (Adapted from [42]).

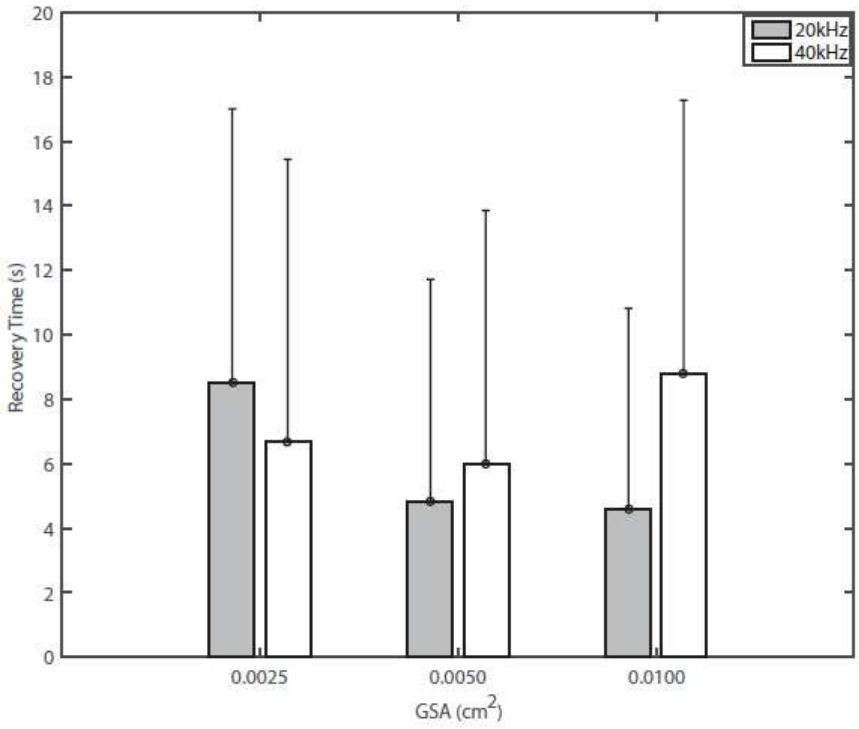

Figure 5. Post-KES recovery time of EMG activity. Gray and white boxes represent the duration between the end of KES block delivery and recovery of EMG activity to 90% of pre-KES block values. Mean recovery times decrease as a function of contact GSA for 20 kHz KES, however the standard deviation is large and the same behavior is not observed with 40 kHz trials. One-way analysis of variance demonstrated no significant difference in recovery times as a function of contact GSAs. (Adapted from [42]).

Materials

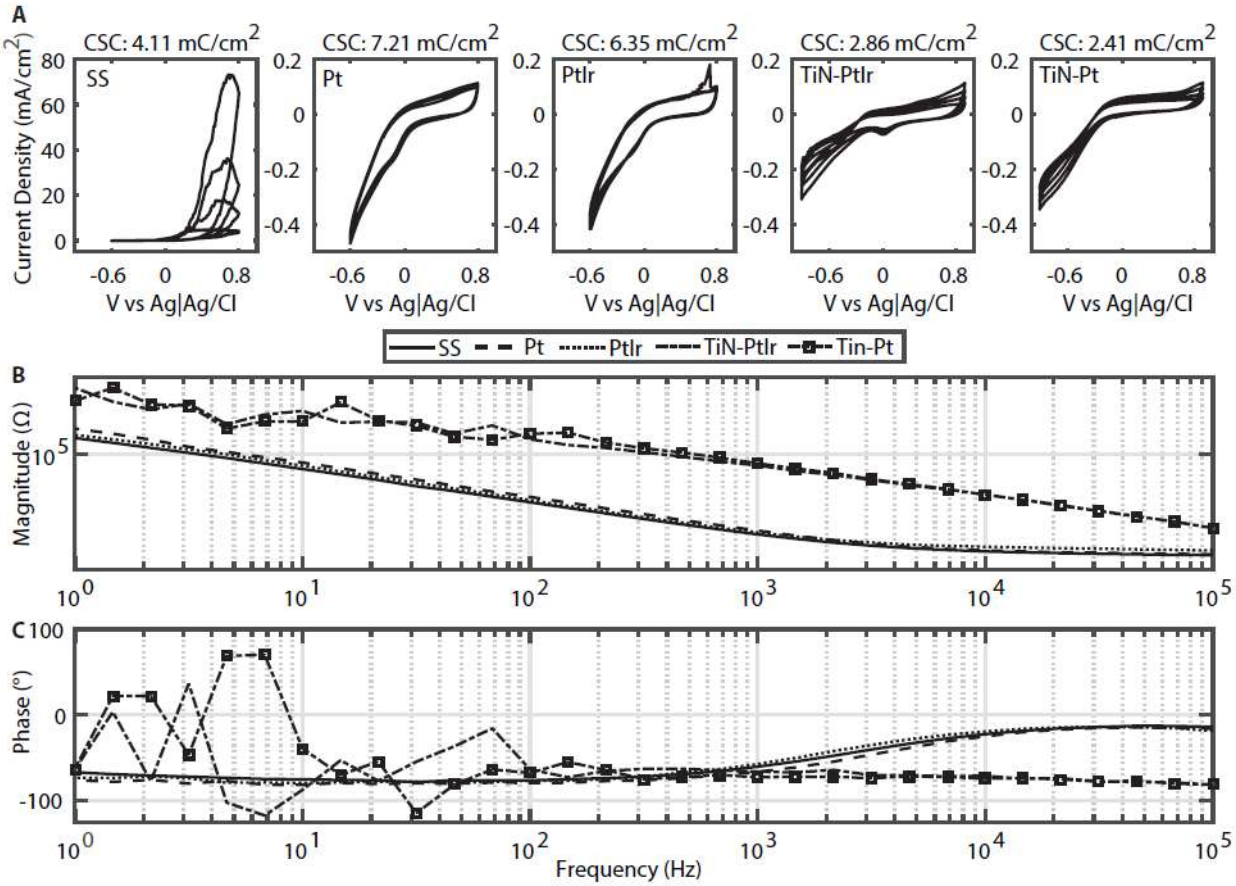

Figure 6. Electrochemical characterization of electrodes. (A) Five voltammograms and corresponding cathodic CSC are depicted for each contact material evaluated. Cathodic CSC is average of all five voltammograms per material were averaged to calculate the cathodic CSC. Representative electrochemical impedance magnitude (B) and phase angle (C) are shown for each material. Electrode material does not impact KES nerve block thresholds. (Adapted from [43]).

Electrochemical characteristics of electrodes

Electrochemical characterization of electrodes provides valuable information about the electrode stability and the response of electrodes to different stimulation waveforms. We performed CV measurements to quantify the cathodic CSC and EIS measurements to evaluate the frequency response and electrochemical reactions for each material. Figure 6A shows the cyclic voltammograms for each material evaluated. With the exception of SS, all other electrode materials depict both Faradaic and non-Faradaic reactions as the potential is swept, with a greater Faradaic response by the Pt and PtIr

electrodes and a greater non-Faradaic response displayed by the TiN electrodes. The voltammogram for SS depicts the presence of a developing oxide layer on the electrode surface and early stages of pitting, suggesting the onset of metal corrosion. In addition, SS presents increased water oxidation as observed by the significantly increased positive current. The electrochemical spectra for all electrode materials are displayed in Fig. 6B-C with mean and standard deviation values at relevant KES frequencies shown in Table III. The access (or tissue) impedance for each material was taken at 100 kHz. The impedance magnitude decreases across the frequency spectrum for all materials. Interestingly, although the electrochemical surface area of TiN coated electrodes is greater, the impedance magnitude is significantly higher than planar, noncoated electrodes (discussed later). The decreased phase shift in the phase spectra of SS, Pt, and PtIr suggests that at high frequencies (>1 kHz), the solution (tissue) access resistance dominates. The nearly stationary phase shift observed for TiN coated electrodes suggests the presence of a double-layer and thus non-Faradaic charge injection mechanisms throughout the entire spectrum. KES nerve block thresholds (Fig. 8) demonstrate no statistically significant dependence upon the electrode contact material at either frequency.

Table III
Impedance characteristics (Adapted from [43]).

Material	20 kHz	40 kHz	Access (100 kHz)
SS (Ω)	267.5 ± 89.4	249.8 ± 53.1	238.3 ± 78.6
Pt (Ω)	282.7 ± 92.4	262.0 ± 72.4	248.2 ± 36.6
PtIr (Ω)	405.3 ± 62.6	375.6 ± 53.9	349.7 ± 52.1
TiN-Pt/Ir (Ω)	4755.1 ± 432.5	2381.8 ± 395.6	1184.2 ± 119.5
TiN-Pt (Ω)	4236.6 ± 714.1	2259.1 ± 463.7	1120.9 ± 108.3

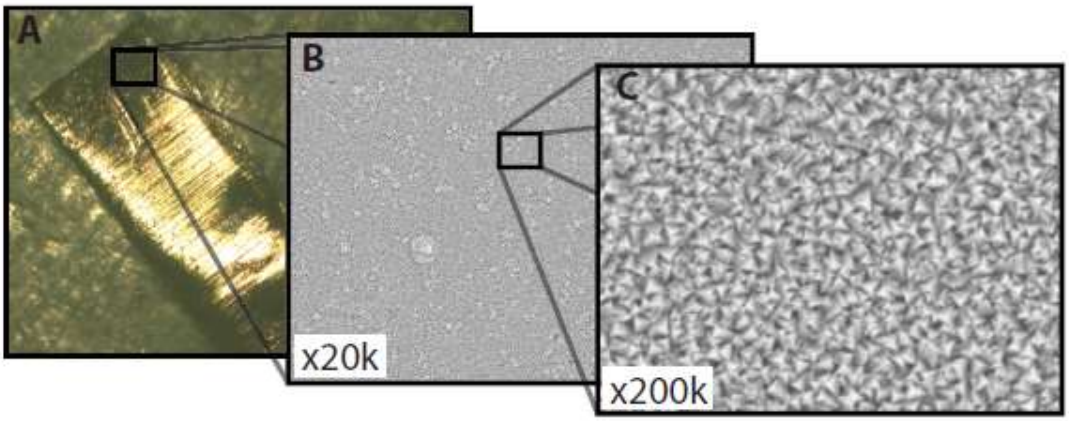

Fig. 7. Surface composition of TiN coated electrodes. (A) Light microscope image of TiN-PtIr electrode. Scanning electron microscope images (B: x20k, C: x200k) of TiN-PtIr electrode surface. Increased electrochemical surface area of TiN coating is visible. (Adapted from [43]).

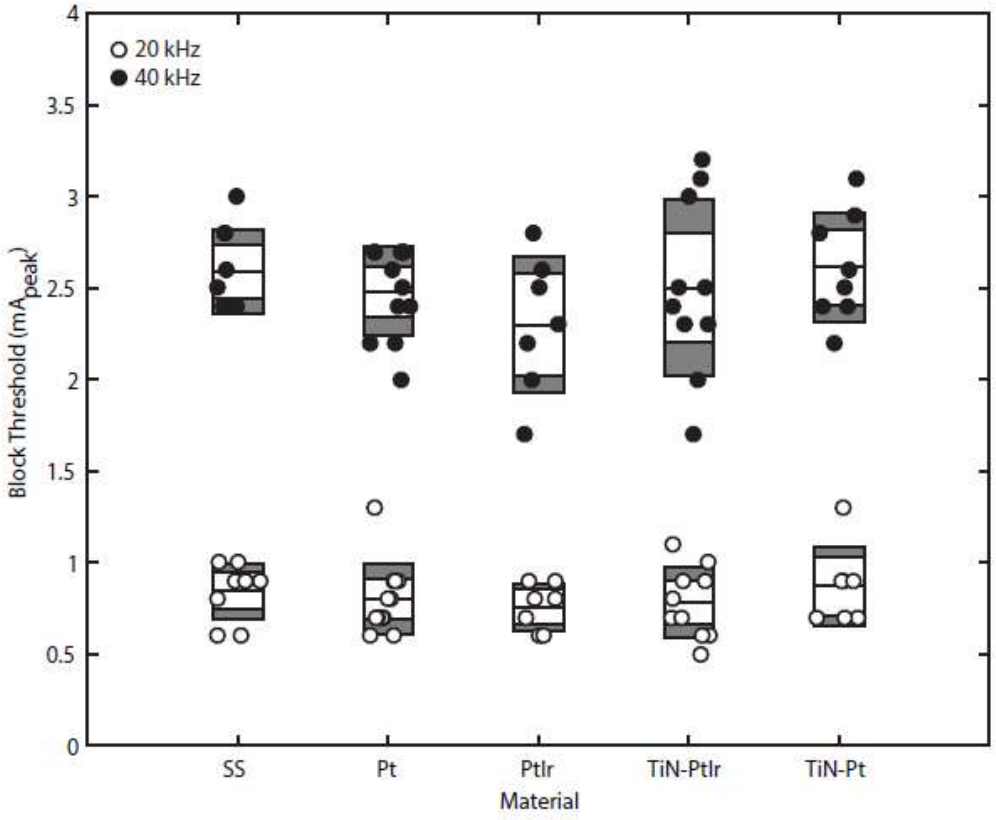

Figure 8. KES block thresholds as a function of electrode contact material for 20 and 40 kHz KES nerve block. Each dot represents an individual trial. No statistically significant difference was observed between block thresholds with a given material at either 20 kHz or 40 kHz (Tukey-Kramer multiple comparison test, $\alpha = 0.05$). (Adapted from [43]).

Electrode material does not impact KES nerve block thresholds

KES nerve block thresholds (Fig. 8) demonstrate no statistically significant dependence upon the electrode contact material at either frequency. In contrast, the average power consumption for TiN coated electrodes is higher with respect to non-coated electrodes, primarily due to the increased impedance magnitudes displayed in the EIS measurements (Fig. 6B).

Electrode material does not alter post-KES nerve block characteristics

The clinical utility of KES nerve block may be affected by the onset response, changes in normal nerve conduction, as well as recovery of normal conduction after KES is turned off. The onset response durations (Fig. 9) were quantified as a function of KES frequency and contact material. No statistically significant difference was observed for the onset duration as a function of electrode contact material. Quantification of pre- and post-KES evoked EMG latencies (not shown) demonstrate no difference in nerve conduction from application of 60 s of KES.

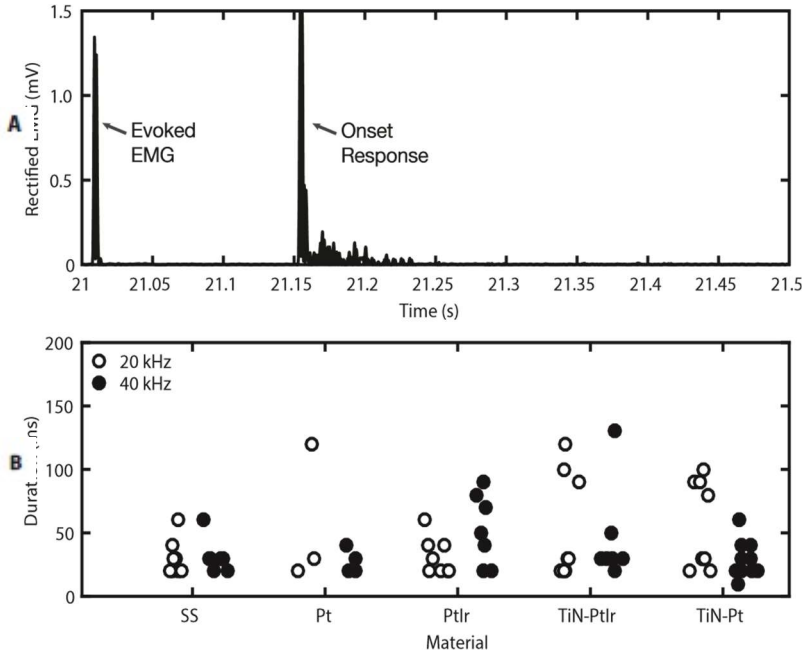

Figure 9. Rectified EMG onset artifact and durations. (A) Rectified EMG onset artifact consists of a large, high-frequency transient spike in measured EMG activity followed by a brief period of spontaneous activation, followed by complete KES nerve block. (B) The width of the windowed rectified EMG onset artifact is used to represent the duration of the onset artifact as a function of contact material and KES frequency. No statistically significant difference was observed between block thresholds with a given material at either 20 kHz or 40 kHz (Tukey-Kramer multiple comparison test, $\alpha = 0.05$). (Adapted from [43]).

CHAPTER 4

DISCUSSION

Geometric Surface Area

Interest and clinical availability of bioelectronic medicines have significantly grown in the past decade mostly due to the initiatives started by for-profit and non-profit entities. At the root of many of these initiatives is the ability to interface with the nervous system - in particular with the peripheral nervous system with the goal of monitoring and treating a variety of clinical conditions. KES nerve block offers a promising new approach for bioelectronic medicines - providing both temporal and spatial control of peripheral nerve activity. A significant number of questions remain to be answered to ensure safe and effective implementation of KES nerve block in clinical therapies - including but not limited to the optimal electrode specifications.

In the present study, preparations of the anesthetized rat tibial nerve were used to evaluate the effects of increasing GSA on KES nerve block thresholds. Increasing GSA was achieved by increasing the length of the electrode contacts while the width was fixed. The effect of three different contact lengths (Table II) on KES nerve block thresholds were evaluated with KES frequencies of 20 and 40 kHz. Our results demonstrate that KES nerve block thresholds are inversely related to the electrode contact GSA (Figure 2), and that the magnitude of this inverse relationship increases at higher KES frequencies. The inverse relationship between contact GSA and block thresholds is likely due to multiple factors - such as lower impedance magnitudes and increased electric field uniformity. Increasing GSA provides for lower thresholds for KES nerve block but has no statistically significant and observable effect on the onset artifact duration, recovery, or the nerve conductivity (Figs. 3, 4).

One observation of the experimental data presented here (Figs. 2, 3, 4) is the wide range of variability in computed metrics. These experiments were performed with acute preparations which typically demonstrate a wide range of variability. This variability is inherently tied to acute experiments due to differences in the electrode-tissue interface

resulting in different input-output relationships [46]. It is speculated that this variability will decrease significantly in chronic experimental evaluation. For example, the KES block thresholds (Fig. 2), although well within the published range of block thresholds at each KES frequency, might present a significantly tighter variance on a per-nerve basis once the variation of electrode placement is compensated by fibrous tissue encapsulation . It is also possible that the low levels of direct current contamination measured in our experiments contributed to the observed variability. For example, the reduction in post-KES EMG activity may be due to localized damage to axonal structures and requires histological examination. Previous investigations have been reported on the use of blocking capacitors and/or inductors to minimize direct current contamination of KES waveforms [47]. We did not employ these methods but did characterize the contamination. Our experience with blocking capacitors suggests that direct current contamination is reduced during delivery of KES. However, the capacitors discharge through the neural tissue when KES delivery is turned off, significantly damaging the underlying neural tissues. Large inductors (>5 H) provide one solution to the discharging of blocking capacitors and direct current contamination [48], but are clinically impractical.

Although not assessing contact GSA, other investigations have characterized the effects of electrode geometry, specifically spacing between electrode contacts on the KES nerve block threshold as well as the onset artifact. Ackermann et al [17] investigated the effect of inter-pole distance on both KES nerve block thresholds and the onset response with results suggesting that 1 mm between poles is optimal. A number of follow-up investigations by the same group were carried out to reduce the onset response which can last up to 10 s after initiation of KES nerve block [18], [32]. However, this onset artifact duration is in contrast to our findings which demonstrate (Figure 3) that the onset response never exceeded 120 ms [4]. The longer duration onset artifacts published by others using the sciatic-gastrocnemius muscle complex preparation are likely a combination of both the neural onset (milliseconds) and physiological onset (seconds). In this case, the physiological onset is the passive relaxation properties of muscle fibers. The concept of neural vs physiological onset

artifacts is an important factor that should be considered when evaluating the onset response in different neural circuits.

In addition to the short duration onset response, our experimental results demonstrate that recovery after 60 seconds of KES nerve block is nearly instantaneous with significant variability in terms of the magnitude of the recovered EMG response (Fig. 4). The variability could be due to the extremely low levels of direct current measured in our experiments, however we stimulated the nerve distal to the KES nerve block cuff electrode to validate that KES block was local to the site of the block cuff electrode and not neuromuscular fatigue or depletion block [47]. In all our trials, recovery of EMG activity was instantaneous with proximal stimulation evoked EMG measured within less than one second of turning off KES nerve block. Analysis of post-KES block EMG activity suggests that evoked EMG (resulting from nerve conduction recovery) returns to 90% of pre-KES EMG magnitude within an average of 10 seconds (Fig. 5). These post-KES recovery characteristics are similar to previous reports [49], but in conflict with others [36]. In the latter investigation, complete KES nerve block was observed up to 10 seconds after turning off KES. Although the study states the use of an electrode to stimulate the nerve distal to the block site, complete trials are not shown and twitches in response to distal stimulation are absent from force transducer measurements ([36] Figs. 2-4), suggesting that the results maybe an artifact of neuromuscular depletion or fatigue block, rather than a true conduction block localized to the KES electrode.

Materials

KES nerve block holds great promise as a new approach for modulating the nervous system through peripheral and autonomic nerves. Successful translation of KES nerve block therapies requires investigation of a variety of unanswered questions. The present study evaluated the effect of different electrode materials, and thus different charge injection mechanisms, on KES nerve block characteristics. Electrochemical studies were conducted to understand the charge injection mechanisms and electrical

characteristics of each material. In vivo experiments were conducted on the rat tibial nerve with gastrocnemius muscle EMG as a readout for KES nerve block.

Our results demonstrate that KES nerve block thresholds (Fig. 8) and onset artifact duration (Fig. 9) do not differ with different electrode materials. These results further support findings by others suggesting that the electrode geometry (inter-pole distance) is the critical factor for minimizing the block threshold and onset response [50], [22].

The contacts used in this investigation were made of Pt or PtIr, both of which have received significant attention by the neural stimulation community [51]–[53]. Pt and PtIr both utilize both faradaic and non-Faradaic charge injection mechanisms, with the contribution of each mechanism depending upon the current density and the pulse width. In the case of KES waveforms, where the pulse widths are extremely short, the non-Faradaic mechanisms dominate. The lack of a significant effect of materials on KES nerve block characteristics is likely due to the dominating electrochemical mechanisms at high frequencies. All evaluated electrode materials show a dependence upon non-Faradaic charge transfer mechanisms at KES frequencies based upon the EIS data (Fig. 6B-C).

A typical concern with KES nerve block is the initial asynchronous activation of the nerve called the onset response. Depending on the neural circuit being modulated, the onset response can be of great concern. In somatic nerves the onset typically represents itself as activation of the muscle and can last up to 10 s, with electrode configurations demonstrated to play a critical role in minimizing the onset response [50], [36]. The onset response characterized in our investigations typically lasted <200 ms (Fig. 9). This disparity is likely due to differences in the true nerve onset measured from the nerve, lasting several milliseconds [4], versus the onset measured through force transduction, which includes the passive relaxation time of the muscle after being asynchronously activity. It remains to be thoroughly investigated how electrodes with penetrating features, such as minimally invasive microneedles [54], might impact the safety, efficacy, and characteristics of KES nerve block.

The biophysical mechanism(s) of KES nerve block are unknown, however multiple computational studies have proposed different mechanisms. One proposed hypothesis is that KES nerve block is achieved via inactivation of sodium channels by membrane depolarization [2], [6], [55]. In contrast, it has been hypothesized that KES leads to elevated levels of potassium channel activation [56]–[58]. This investigation does not speak directly to the existing hypothesized mechanisms, however do suggest that computational investigations can safely ignore electrode material aspects when investigating KES nerve block.

CHAPTER 5

CONCLUSION

KES nerve conduction block is a powerful neuromodulation technique capable of providing fast, effective, and robust block of nerve activity. The results presented in this manuscript demonstrate the dependence of KES nerve block thresholds on GSA and independence of KES nerve block thresholds and post-KES nerve block characteristics on various electrode materials and charge injection mechanisms. These results suggest that the electrode's GSA be maximized and material used for KES nerve block be selected based upon proven track records of chronic stability, long-term safety, and manufacturing methods. For example, Pt/Ir alloys, which primarily utilize non-Faradaic charge injection mechanisms at KES frequencies, may provide chronic stability and safety for both the nerve and electrode.

REFERENCES

[1] L. Joseph and R. J. Butera, “Unmyelinated Aplysia nerves exhibit a nonmonotonic blocking response to high-frequency stimulation.” IEEE Transactions on Neural Systems and Rehabilitation Engineering, vol. 17, no. 6, pp. 537–544, 2009.

[2] K. L. Kilgore and N. Bhadra, “Nerve conduction block utilising highfrequency alternating current,” Medical & Biological Engineering & Computing, vol. 42, no. 3, pp. 394–406, 2004.

[3] L. Joseph and R. J. Butera, “High-frequency stimulation selectively blocks different types of fibers in frog sciatic nerve,” IEEE Transactions on Neural Systems and Rehabilitation Engineering, vol. 19, no. 5, pp. 550–557, 2011.

[4] Y. A. Patel and R. J. Butera, “Differential fiber-specific block of nerve conduction in mammalian peripheral nerves using kilohertz electrical stimulation.” Journal of Neurophysiology, vol. 113, no. 10, pp. 3923–9, 2015.

[5] R. P. Williamson and B. J. Andrews, “Localized electrical nerve blocking,” IEEE Transactions on Biomedical Engineering, vol. 52, no. 3, pp. 362–370, 2005.

[6] N. Bhadra and K. Kilgore, “Block of mammalian motor nerve conduction using high frequency alternating current,” in Conference Proceedings 2nd International IEEE EMBS Conference on Neural Engineering, vol. 10, 2005, pp. 1–3.

[7] N. Bhadra, N. Bhadra, K. Kilgore, and K. J. Gustafson, “High frequency electrical conduction block of the pudendal nerve,” Journal of Neural Engineering, vol. 3, no. 2, pp. 180–187, 2006.

[8] A. Boger, N. Bhadra, and K. J. Gustafson, “Different clinical electrodes achieve similar electrical nerve conduction block.” Journal of Neural Engineering, vol. 10, no. 5, p. 056016, 2013.

[9] E. Lin, K. L. Kilgore, N. Bhadra, and E. A. Lahowetz, “Chronic high-frequency nerve block with an implanted waveform generator,” in International Functional Electrical Stimulation Society Conference, 2007, p. 1.

[10] J. M. Cuellar, K. Alataris, A. Walker, D. C. Yeomans, and J. F. Antognini, “Effect of high-frequency alternating current on spinal afferent nociceptive transmission.” Neuromodulation: Technology at the Neural Interface, vol. 16, no. 4, pp. 318–327, 2013.

[11] M. Camilleri, J. Toouli, M. F. F. Herrera, B. Kulseng, L. Kow, J. P. Pantoja, R. Marvik, G. Johnsen, C. J. Billington, F. G. Moody, M. B. Knudson, K. S. Tweden, M. Vollmer, R. R. Wilson, and M. Anvari, “Intra-abdominal vagal blocking (VBLOC therapy): clinical results with a new implantable medical device,” Surgery, vol. 143, no. 6, pp. 723– 731, 2008.

[12] D. M. Ackermann, N. Bhadra, M. Gerges, and P. J. Thomas, “Dynamics and sensitivity analysis of high-frequency conduction block.” Journal of Neural Engineering, vol. 8, no. 6, p. 065007, 2011.

[13] Y. A. Patel, T. Saxena, R. V. Bellamkonda, and R. J. Butera, “Kilohertz frequency nerve block enhances anti-inflammatory effects of vagus nerve stimulation,” Scientific Reports, vol. 7, p. 39810, 2017.

[14] C. Veraart, W. M. Grill and J. T. Mortimer, "Selective control of muscle activation with a multipolar nerve cuff electrode," in IEEE Transactions on Biomedical Engineering, vol. 40, no. 7, pp. 640-653, July 1993.doi: 10.1109/10.237694

[15] G.E. Loeb, R.A. Peck, Cuff electrodes for chronic stimulation and recording of peripheral nerve activity, Journal of Neuroscience Methods, Volume 64, Issue 1, January 1996, Pages 95-103, ISSN 0165-0270, http://doi.org/10.1016/0165-0270(95)00123-9.

[16] Navarro, X., Krueger, T. B., Lago, N., Micera, S., Stieglitz, T. and Dario, P. (2005), A critical review of interfaces with the peripheral nervous system for the control of neuroprostheses and hybrid bionic systems. Journal of the Peripheral Nervous System, 10: 229–258. doi:10.1111/j.1085-9489.2005.10303.x

[17] D. M. Ackermann, E. L. Foldes, N. Bhadra, and K. L. Kilgore, “Effect of bipolar cuff electrode design on block thresholds in highfrequency electrical neural conduction block,” IEEE Transactions on Neural Systems and Rehabilitation Engineering, vol. 17, no. 5, pp. 469– 477, 2009.

[18] Boger A, Bhadra N, Gustafson KJ. Bladder voiding by combined high frequency electrical pudendal nerve block and sacral root stimulation. Neurourol Urodyn. 2008;27:435–439.

[20] N. Bhadra and K. L. Kilgore, “High-frequency electrical conduction block of mammalian peripheral motor nerve,” Muscle & Nerve, vol. 32, no. 6, pp. 782–790, 2005.

[21] A. Rosenblueth and J. Reboul, “The blocking and deblocking effects of alternating currents on nerve,” American Journal of Physiology Legacy Content, vol. 125, no. 2, pp. 251–264, 1939.

[22] D. M. Ackermann, N. Bhadra, E. L. Foldes, X. F. Wang, and K. L. Kilgore, “Effect of nerve cuff electrode geometry on onset response firing in high-frequency nerve conduction block,” IEEE Transactions on Neural Systems and Rehabilitation Engineering, vol. 18, no. 6, pp. 658–665, 2010.

[23] M. Cattell and R. W. Gerard, “The ”inhibitory” effect of high-frequency stimulation and the excitation state of nerve.” The Journal of Physiology, vol. 83, no. 4, pp. 407–15, 1935.

[24] J. Reboul and A. Rosenblueth, “The action of alternating currents upon the electrical excitability of nerve,” American Journal of Physiology Legacy Content, vol. 125, no. 2, pp. 205–215, 1939.

[25] J. A. Tanner, “Reversible blocking of nerve conduction by alternatingcurrent excitation.” Nature, vol. 195, no. 4842, pp. 712–713, 1962.

[26] M.Woo and B. Campbell, “Asynchronous Firing and Block of Peripheral Nerve Conduction by 20 Kc Alternating Current,” Bulletin of the Los Angeles Neurological Society, vol. 29, p. 87, 1964.

[27] R. Baratta, M. Ichie, S. K. Hwang, and M. Solomonow, “Orderly stimulation of skeletal muscle motor units with tripolar nerve cuff electrode.” IEEE Transactions on Biomedical Engineering, vol. 36, no. 8, pp. 836–843, 1989.

[28] B. R. Bowman and D. R. McNeal, “Response of single alpha motoneurons to high-frequency pulse trains,” Stereotactic and Functional Neurosurgery, vol. 49, no. 3, pp. 121–138, 1987.

[29] C. Tai, J. R. Roppolo, and W. C. de GROAT, “Block of external urethral sphincter contraction by high frequency electrical stimulation of pudendal nerve,” The Journal of urology, vol. 172, no. 5, pp. 2069– 2072, 2004.

[30] J. D. Miles, K. L. Kilgore, N. Bhadra, and E. Lahowetz, “Effects of ramped amplitude waveforms on the onset response of high-frequency mammalian nerve block.” Journal of Neural Engineering, vol. 4, no. 4, pp. 390–398, 2007.

[31] A. Boger, N. Bhadra, and K. J. Gustafson, “Bladder voiding by combined high frequency electrical pudendal nerve block and sacral root stimulation,” Neurourology and Urodynamics, vol. 27, no. 5, pp. 435– 439, 2008.

[32] L. Joseph, B. D. Haeffele, and R. J. Butera, “Conduction block induced by high frequency AC stimulation in unmyelinated nerves.” Annual International Conference of the IEEE Engineering in Medicine and Biology Society, pp. 1719–1722, 2007.

[33] D. M. Ackermann, E. L. Foldes, N. Bhadra, and K. L. Kilgore, “Nerve conduction block using combined thermoelectric cooling and high frequency electrical stimulation,” Journal of Neuroscience Methods, vol. 193, no. 1, pp. 72–76, 2010.

[34] M. Gerges, E. L. Foldes, M. D. Ackermann, N. Bhadra, N. Bhadra, and K. L. Kilgore, “Frequency- and amplitude-transitioned waveforms mitigate the onset response in high-frequency nerve block.” Journal of Neural Engineering, vol. 7, no. 6, p. 066003, 2010.

[35] D. M. Ackermann, E. L. Foldes, N. Bhadra, and K. L. Kilgore, “Conduction block of peripheral nerve using high-frequency alternating currents delivered through an intrafascicular electrode,” Muscle & Nerve, vol. 41, no. 1, pp. 117–119, 2010.

[36] D. M. Ackermann, N. Bhadra, E. L. Foldes, and K. L. Kilgore, “Conduction block of whole nerve without onset firing using combined high frequency and direct current,” Medical & Biological Engineering & Computing, vol. 49, no. 2, pp. 241–251, 2011.

[37] M. D. Ackermann, N. Bhadra, E. L. Foldes, and K. L. Kilgore, “Separated Interface Nerve Electrode Prevents Direct Current Induced Nerve Damage,” Journal of Neuroscience Methods, vol. 201, no. 1, pp. 173–176, 2011.

[38] D. Michael Ackermann, C. Ethier, E. L. Foldes, E. R. Oby, D. Tyler, M. Bauman, N. Bhadra, L. Miller, and K. L. Kilgore, “Electrical conduction block in large nerves: Highfrequency current delivery in the nonhuman primate,” Muscle & Nerve, vol. 43, no. 6, pp. 897–899, 2011.

[39] H. Liu, L. Zhu, S. Sheng, L. Sun, H. Zhou, H. Tang, and T. Qiu, “Post stimulus effects of high frequency biphasic electrical current on a fibre’s conductibility in isolated frog nerves.” Journal of Neural Engineering, vol. 10, no. 3, p. 036024, 2013.

[40] G. Yang, Z. Xiao, J. Wang, B. Shen, J. R. Roppolo, W. C. de Groat, and C. Tai, “Post-stimulation block of frog sciatic nerve by high-frequency (kHz) biphasic stimulation,” Medical & Biological Engineering & Computing, pp. 1–9, 2016.

[42] Patel Y.A, Kim B.S, Rountree W.S, Butera R.J, “Kilohertz Electrical Stimulation Nerve Conduction Block: Effects of electrode surface area.” In press IEEE Transactions on Neural Systems & Rehabilitation Engineering,2016.

[43] Patel Y.A, Kim B.S, Rountree W.S, Butera R.J (2016), Kilohertz Electrical Stimulation Nerve Conduction Block: Effects of electrode materials. Under review

[44] Normal rat ringer’s solution. [Online]. Available: http://cshprotocols.cshlp.org/content/2012/2/pdb.rec068312.full?text only=tru

[45] H. Schmalbruch, “Fiber composition of the rat sciatic nerve,” The Anatomical Record, vol. 215, no. 1, pp. 71–81, 1986.

[46] W. M. Grill and J. T. Mortimer, “Stability of the input-output properties of chronically implanted multiple contact nerve cuff stimulating electrodes,” IEEE Transactions on Rehabilitation Engineering, vol. 6, no. 4, pp. 364–373, 1998.

[47] M. Franke, N. Bhadra, N. Bhadra, and K. Kilgore, “Direct current contamination of kilohertz frequency alternating current waveforms,” Journal of Neuroscience Methods, vol. 232, no. 2014, pp. 74–83, may 2014.

[48] K. L. Kilgore and N. Bhadra, “Reversible nerve conduction block using kilohertz frequency alternating current,” Neuromodulation: Technology at the Neural Interface, vol. 17, no. 3, pp. 242–254, 2014.

[49] H. Liu, L. Zhu, S. Sheng, L. Sun, H. Zhou, H. Tang, and T. Qiu, “Post stimulus effects of high frequency biphasic electrical current on a fibre’s conductibility in isolated frog nerves.” Journal of Neural Engineering, vol. 10, no. 3, p. 036024, 2013.

[50] C. Tai, D. Guo, J. Wang, J. R. Roppolo, and W. C. de Groat, “Mechanism of conduction block in amphibian myelinated axon induced by biphasic electrical current at ultra-high frequency.” Journal of Computational Neuroscience, vol. 31, no. 3, pp. 615–23, 2011.

[51] S. F. Cogan, P. R. Troyk, J. Ehrlich, and T. D. Plante, “In Vitro Comparison of the Charge-Injection Limits of Activated Irirdium Oxide (AIROF) and Platimum-Irirdium Microelectrodes,” IEEE Transactions on Biomedical Engineering, vol. 52, no. 9, pp. 1612–1613, 2005.

[52] E. K. Brunton, B. Winther-Jensen, C. Wang, E. B. Yan, S. Hagh Gooie, A. J. Lowery, and R. Rajan, “In vivo comparison of the charge densities required to evoke motor responses using novel annular penetrating microelectrodes.” Frontiers in Neuroscience, vol. 9, no. May, p. 265, 2015.

[53] D. Kumsa, E. M. Hudak, F. W. Montague, S. C. Kelley, D. F. Untereker, B. P. Hahn, C. Condit, M. Cholette, H. Lee, D. Bardot, and P. Takmakov, “Electrical neurostimulation with imbalanced waveform mitigates dissolution of platinum electrodes,” Journal of Neural Engineering, vol. 13, no. 5, p. 054001, 2016. [Online]. Available: http://stacks.iop.org/174-2552/13/i=5/a=054001?key=crossref.4ee00c0857dde0c1a0a171d55c7f06b1

[54] Y. A. Patel, A. Willsie, I. P. Clements, R. Aguilar, S. Rajaraman, and R. J. Butera, “Microneedle cuff electrodes for extrafascicular peripheral nerve interfacing,” in 38th Annual International Conference of the IEEE Engineering in Medicine and Biology Society, 2016, pp. 1741–1744.

[55] N. Bhadra, E. A. Lahowetz, S. T. Foldes, and K. L. Kilgore, “Simulation of high-frequency sinusoidal electrical block of mammalian myelinated axons,” Journal of Computational Neuroscience, vol. 22, no. 3, pp. 313–326, 2007.

[56] C. Zhang, X, Tai, “Mechanism of nerve conduction block induced by high-frequency biphasic electrical currents,” IEEE Transactions on Biomedical Engineering, vol. 53, no. 12, pp. 1–19, 2006.

[57] C. Tai, W. C. D. Groat, and J. R. Roppolo, “Simulation analysis of conduction block in unmyelinated axons induced by high-frequency biphasic electrical currents.” IEEE Transactions on Biomedical Engineering, vol. 52, no. 7, pp. 1323–1332, 2005.

[58] H. Liu, J. R. Roppolo, W. C. De Groat, and C. Tai, “The role of slow potassium current in nerve conduction block induced by high-frequency biphasic electrical current,” IEEE Transactions on Biomedical Engineering, vol. 56, no. 1, pp. 137–146, 2009.